ELSEVIER

Computational Materials Science 9 (1998) 329–336

COMPUTATIONAL MATERIALS SCIENCE

Phase field formulations for modeling the Ostwald ripening in two-phase systems [1]

Danan Fan [a,*], Long-Qing Chen [b], S.P. Chen [a], Peter W. Voorhees [c]

[a] *Theoretical Division, MS B262, Los Alamos National Laboratory, Los Alamos, NM 87545, USA*
[b] *Department of Materials Science and Engineering, The Pennsylvania State University, University Park, PA 16802, USA*
[c] *Department of Materials Science and Engineering, Northwestern University, Evanston, IL 60208, USA*

Received 17 June 1997; accepted 11 August 1997

Abstract

Phase field formulations have been constructed for modeling Ostwald ripening in two-phase systems. The microstructural evolution and the kinetics of Ostwald ripening were studied by numerically solving the time-dependent Ginzburg–Landau (TDGL) equations. The simulated microstructures are in a striking resemblance with experimental observations. The shape accommodation of second phase particles occurs as the volume fraction increases. It was observed that these two-phase systems reach the steady state or scaling state after a short transient time and the scaling functions are independent of time for all volume fractions of the second phase. The kinetics of Ostwald ripening in a two-phase mixture have been studied over a range of volume fractions of the coarsening phase. It was found that the coarsening kinetics of second phase particles follows the power growth law $R_t^m - R_0^m = kt$ with $m = 3$, which is independent of the volume fraction of the coarsening phase. The kinetic coefficient k increases significantly as the volume fraction of the coarsening phase increases. © 1998 Published by Elsevier Science B.V.

1. Introduction

Ostwald ripening is a process related to the coarsening of one phase dispersed in the matrix of another. The average size of the particles of the dispersed phase increases during coarsening due to diffusion through the matrix phase, and their total number decreases. The driving force for the process is the reduction of the total interfacial area and thus of the total energy of the system. Ostwald ripening is a common microstructural evolution process observed in a wide variety of two-phase systems and has been extensively studied because of its practical importance in casting, welding processes, liquid phase sintering and in precipitation hardening alloys.

Modern theories of Ostwald ripening are based on the classical work of Lifshitz and Slyozov and Wagner [1,2], which is known as LSW theory. In LSW theory, the problem of coarsening kinetics was solved by assuming a steady-state diffusion field, an infinitesimally dilute second phase, spherical particles and by assuming that particles interact only indirectly with each other through a mean field provided by the interparticle matrix. There are three equations necessary to describe the ripening kinetics of a two-phase system: a kinetic equation describing the growth or shrinkage rate of a particle of a given size,

[1] Paper presented at the Materials Research Society, Spring 1997 meeting, symposium on "Computational Materials Science at the Mesoscale".

* Corresponding author.

0927-0256/98/$19.00
PII S0927-0256(97)00158-4

a continuity equation describing the temporal evolution of a particle size distribution function, and a mass conservation equation. Based upon assumptions made and solutions to these equations, the LSW theory predicted a power growth law $R_t^m - R_0^m = kt$ with $m = 3$ and a grain size distribution function in steady state for diffusion controlled coarsening. Since interparticle diffusional interactions are neglected in LSW theory, this theory is valid only in the physically unrealistic limit of zero volume fraction of the second phase. This is one of the reasons given to explain the fact that the experimental results do not agree with the size distribution function [3,4] obtained from LSW theory.

Many efforts have been made to include a finite volume fraction of the second phase using a variety of techniques, including statistical mechanical theories, mean field theories and numerical simulations [5–10] for 3D and [11–13] for 2D. Despite the different physical bases and features of these models and theories, most of them assume that the coarsening particles are spherical in shape to avoid the complexity of irregular geometry. However, this assumption cannot remain valid at high volume fractions, where the particles within the microstructure become crowded and exhibit shape accommodation. Shape accommodation results in the non-uniform distribution of curvature over the particle interface. At very high volume fractions of coarsening particles, crowded particles develop flattened sides, curved edges and rounded vertices or corners. The effects of geometrical complexity at high volume fractions have not been included in the theoretical treatments. As a result, the behaviors of Ostwald ripening in the high volume fraction regime remain poorly understood. Since Ostwald ripening is a moving boundary problem, it is very difficult to solve analytically in the high volume fraction regime. As a result, computer simulations [14] play an important role in understanding Ostwald ripening behavior.

Therefore, it is the purpose of this paper to construct a computer modeling methodology using the continuum field theory for studying Ostwald ripening behavior over a range of volume fractions of the coarsening phase. The authors have employed similar methodologies to study the grain growth in single phase systems [15,16] and the microstructural evolution in two-phase polycrystalline materials [17,18].

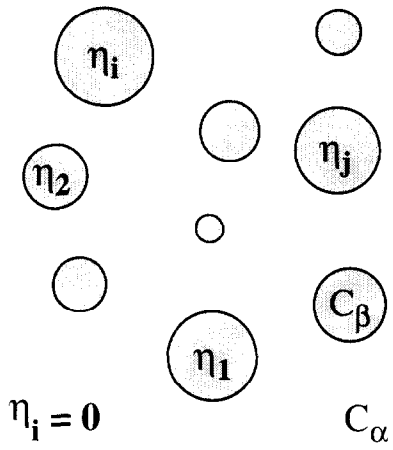

Fig. 1. A schematic microstructure of a two-phase system with second phase particles dispersed in a matrix phase. The orientation field variables η_1, ..., η_j represent different crystallographic orientations of the second phase grains in space. All orientation fields are zero in liquid or disordered (matrix) phase. The equilibrium compositions or solubilities are C_α for the matrix phase and C_β for the second phase, respectively.

One of the main advantages of this model is that the complexity of microstructural evolution and long-range diffusion in two-phase materials can be automatically taken into account. Computer simulations using this formulation allow one not only to monitor the detailed temporal microstructure evolution during Ostwald ripening but also to obtain all the information about the average grain size and size distributions. We will focus on the microstructural scaling and the kinetics of Ostwald ripening in this paper. The effect of the volume fraction of second phase on size distributions will be presented in separate publications.

2. The phase field formulation

2.1. Description of a microstructure using phase fields

A schematic microstructure of one phase particles dispersed in the continuous matrix of another is shown in Fig. 1. In this microstructure, there are different crystallographic orientations in the space for second phase particles or grains. The solubilities

or equilibrium concentrations are C_α and C_β for the matrix phase and second phase, respectively. According to the continuum field theory, we define a set of continuous field variables,

$$\eta_1(r), \eta_2(R), \ldots, \eta_p(r), C(r)$$

where p is the number of possible orientations of the second phase grains in space and η_i $(i = 1, \ldots, p)$ are orientation field variables with each orientation field representing grains of a given crystallographic orientation in space, r is the position in the space. These variables change continuously in the space and assume continuous values ranging from -1.0 to 1.0. For example, a value of 1.0 for $\eta_1(r)$ with all other orientation variables being 0.0 means that the material at position r belongs to the grain with the crystallographic orientation labeled as 1; a value of -1.0, indicates that the grain at position r is 180°-rotation related to orientation 1. At the grain boundary region between two grains with orientation 1 and 2, $\eta_1(r)$ and $\eta_2(r)$ will have absolute values intermediate between 0.0 and 1.0. All orientation field variables are zero in the matrix phase, which simulate the liquid or disordered phase. $C(r)$ is the composition field which takes the value of C_α within the matrix phase and C_β within a second phase grain. $C(r)$ has intermediate values between C_α and C_β at the interfacial region between the matrix phase and a second phase grain. Therefore, with the set of field variables, we can completely describe a microstructure with the second phase particles dispersed in the matrix phase.

2.2. Energetics of a two-phase system

Within the diffuse-interface field theory, the total free energy of an inhomogeneous system can be written as:

$$F = \int \left[f_0\big(C(r); \eta_1(r), \eta_2(r), \ldots, \eta_p(r)\big) + \frac{\kappa_C}{2}(\nabla C(r))^2 + \sum_{i=1}^{p} \frac{\kappa_i}{2}(\nabla \eta_i(r))^2 \right] \mathrm{d}^3 r \quad (1)$$

where ∇C and $\nabla \eta_i$ are gradients of concentration and orientation fields, κ_C and κ_i are the corresponding gradient energy coefficients, and f_o is the local free energy density which, in this work, is,

$$f_0 = f_1(C) + \sum_{i=1}^{p} f_2(C, \eta_i) + \sum_{i=1}^{p} \sum_{j \neq i}^{p} f_3(\eta_i, \eta_j) \quad (2)$$

in which

$$f_1(C) = -(A/2)(C - C_\mathrm{m})^2 + (B/4)(C - C_\mathrm{m})^4 + (D_\alpha/4)(C - C_\alpha)^4 + (D_\beta/4)(C - C_\beta)^4,$$

$$f_2(C, \eta_i) = -(\gamma/2)(C - C_\alpha)^2(\eta_i)^2 + (\delta/4)(\eta_i)^4,$$

$$f_3(\eta_i, \eta_j) = (\varepsilon_{ij}/2)(\eta_i)^2(\eta_j)^2$$

where C_α and C_β are the solubilities in the matrix phase and the second phase respectively, $C_\mathrm{m} = (C_\alpha + C_\beta)/2$, A, B, D_α, D_β, γ, δ, and ε_{ij} are phenomenological parameters. A main requirement for f_0 is that it has $2p$ degenerate minima at equilibrium concentration C_β to distinguish the $2P$ orientation differences of the second phase grains in space. The parameters are chosen in such a way that f_0 has $2p$ degenerate minima with equal depth located at $(\eta_1, \eta_2, \ldots, \eta_p) = (1, 0, \ldots, 0), (0, 1, \ldots, 0), \ldots, (0, 0, \ldots, 1)$ at the equilibrium concentration C_β. This requirement ensures that each point in space can only belong to a grain with a given orientation of a given phase. In the matrix phase, all orientation field variables are zero. The justification for using such a free energy model in the study of coarsening was discussed previously [15–18].

The energy of a planar grain boundary, σ_gb, between a grain of orientation i and another grain of orientation j for two second phase grains, can be written as follows,

$$\sigma_\mathrm{gb} = \int_{-\infty}^{+\infty} \left[\Delta f(\eta_i, \eta_j, C) + \frac{\kappa_C}{2}\left(\frac{\mathrm{d}C}{\mathrm{d}x}\right)^2 + \frac{\kappa_i}{2}\left(\frac{\mathrm{d}\eta_i}{\mathrm{d}x}\right)^2 + \frac{\kappa_j}{2}\left(\frac{\mathrm{d}\eta_j}{\mathrm{d}x}\right)^2 \right] \mathrm{d}x \quad (3)$$

in which

$$\Delta f(\eta_i, \eta_j, C) = f_0(\eta_i, \eta_j, C) - f_0(\eta_{i,e}, \eta_{j,e}, C_\beta) - (C - C_\beta)\left(\frac{\partial f_0}{\partial C}\right)_{\eta_{i,e}, \eta_{j,e}, C_\beta} \quad (4)$$

where $f_0(\eta_{i,e}, \eta_{j,e}, C_\beta)$ represents the free energy density minimized with respect to η_i and η_j at the equilibrium composition of the second phase C_β.

Similarly, the interphase boundary energy between the matrix phase and a second phase grain with orientation i is given by

$$\sigma_{\text{int}} = \int_{-\infty}^{+\infty} \left[\Delta f(\eta_i, C) + \frac{\kappa_C}{2} \left(\frac{\mathrm{d}C}{\mathrm{d}x} \right)^2 + \frac{\kappa_i}{2} \left(\frac{\mathrm{d}\eta_i}{\mathrm{d}x} \right)^2 \right] \mathrm{d}x \tag{5}$$

where

$$\Delta f(\eta_i, C) = f_0(\eta_i, C) - f_0(\eta_{i,e}, C_\beta) - (C - C_\beta) \left(\frac{\partial f_0}{\partial C} \right)_{\eta_{i,e}, C_\beta}. \tag{6}$$

In this case, all other orientation field variables are zero.

2.3. The kinetic equations

By defining orientation and composition field variables, the kinetics of coupled grain growth can be described by their spatial and temporal evolution. In the present model, the evolution kinetics of these field variables are described by the generalized time-dependent Ginzburg–Landau (TDGL) equations:

$$\frac{\mathrm{d}\eta_i(r, t)}{\mathrm{d}t} = -L_i \frac{\delta F}{\delta \eta_i(r, t)}, \quad i = 1, 2, \ldots, p, \tag{7a}$$

$$\frac{\mathrm{d}C(r, t)}{\mathrm{d}t} = \nabla \left\{ D \nabla \left[\frac{\delta F}{\delta C(r, t)} \right] \right\}, \tag{7b}$$

where L_i and D are kinetic coefficients related to grain boundary mobilities and atomic diffusion coefficients, t is time, and F is the total free energy given in Eq. (1). The difference between kinetic equations for orientation field variables $\eta_i(r)$ and concentration field $C(r)$ comes from the fact that $C(r)$ is a conserved field, due to the requirement of the mass conservation at all times in a system, which is governed by the Cahn–Hilliard equation (Eq. (7b)). The orientation fields are non-conserved variables whose evolutions are dependent on the Allen–Cahn equation (Eq. (7a)).

Substituting the free energy functional F in (1) into the kinetic equation (Eqs. (7a) and (7b)) gives

$$\frac{\mathrm{d}\eta_i}{\mathrm{d}t} = -L_i \left[\frac{\partial f_0}{\partial \eta_i} - \kappa_i \nabla^2 \eta_i \right], \quad i = 1, 2, \ldots, p, \tag{8a}$$

$$\frac{\mathrm{d}C}{\mathrm{d}t} = \nabla \left\{ D \nabla \left[\frac{\partial f_0}{\partial C} - \kappa_C \nabla^2 C \right] \right\}. \tag{8b}$$

The microstructural evolution of Ostwald ripening can be studied by numerically solving the above coupled kinetic equations.

3. Numerical simulations

To study Ostwald ripening, we chose a set of 30 orientation variables and a concentration field to characterize microstructures. A 2D 512×512 square system was employed. The phenomenological parameters were chosen to give the energetic condition that the liquid phase or matrix phase totally wets the solid phase or coarsening phase, i.e., the ratio of grain boundary energy with interfacial energy is larger than 2.0. We assumed the following phenomenological parameters: $C_\alpha = 0.05$, $C_\beta = 0.95$, $C_m = (C_\alpha + C_\beta)/2 = 0.5$, $A = 2.0$, $B = 1.0$, $D_\alpha = D_\beta = 1.2$, $\gamma = 2.0$, $\delta = 1.0$, and $\varepsilon_{ij} = 3.0$. The gradient coefficients were chosen as: $\kappa_i = \kappa_j = \kappa_C = 2.0$. These parameters give an energetic ratio $\sigma_{gb}/\sigma_{in} = 2.14$, which satisfies the total wetting condition. The kinetic equations were discretized by the explicit method. The grid size along both Cartesian coordinate axes, Δx, was chosen to be 2.0, and the time step for integration, $\Delta t = 0.1$. Periodic boundary conditions were applied. The diffusivities and mobilities were assumed to be the same for both phases.

Computer simulations were started from a liquid or disordered phase, i.e., a phase with small random values for all field variables (± 0.001) and the average concentration for the composition field with the thermal noises. This ensures the desired volume fractions and the volume conservation. After the quench, grains of the coarsening phase will spontaneously nucleate from the liquid or disordered phase.

The nucleation process was completed within 1500 time steps. Allowing enough time to relax system to the steady state (5000 time steps), the kinetic data for Ostwald ripening and size distributions were extracted from the simulated microstructures. At 5000 time step, there are about 600 grains or particles in the 25% coarsening phase system and about 700 grains in high volume fraction systems. The simulations were stopped when there are about 100 grains left in the 25% volume fraction system and about 200 left in high volume fraction systems.

The typical simulated microstructures with 25%, 50%, 75%, and 90% volume fractions of second phase are shown in Fig. 2. In these microstructures, bright phase is the coarsening phase or solid phase, and the dark phase represents the matrix phase. It can be seen that at a low volume fraction (25%), the coarsening grains are almost perfect spheres and the coarsening is solely controlled by the interparticle diffusion through the matrix phase. At 50% of the coarsening phase, coalescence between coarsening phase grains is observed, which is a result of a finite number of orientation variables were employed in simulations, and most of the grains still keep the spherical shape. However, at 75% volume fraction, coarsening phase grains in microstructures become crowded and the shapes of grains start to depart from being spherical due to the shape accommodation. The microstructures with volume fractions larger than 90% are comprised of grains with flattened sides, curved edges and rounded vertices or corners. In all cases, the coarsening phase grains are wetted by the matrix phase because of the energetic condition.

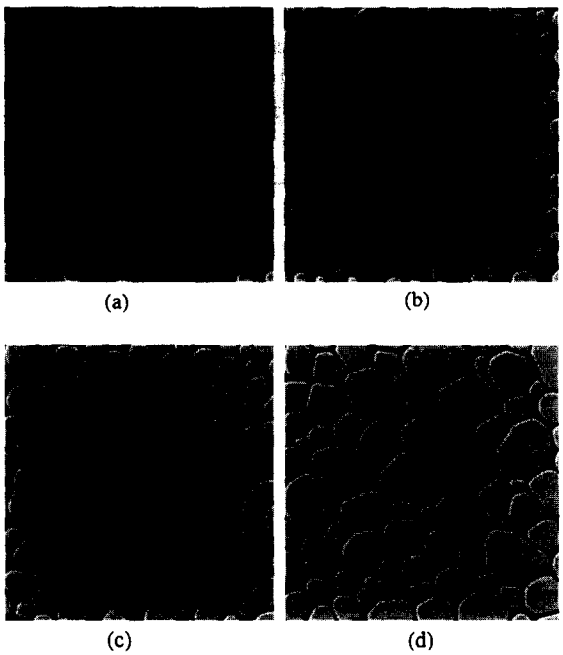

Fig. 2. The simulated microstructures of Ostwald ripening in 2D two-phase systems. The system size is 512×512. The initial microstructure is a liquid. (a) 25% of the second phase; (b) 50% of the second phase; (c) 75% of the second phase; and (d) 90% of the second phase.

Since all theoretical analyses assume a quasi-static diffusion field, it is necessary to examine if these systems reach the steady state or scaling regime. A common method used to study the scaling behavior of a system is to examine the structure function $S(\boldsymbol{k}, t)$ [19–21]. In a two phase system, the correlation function of the concentration field $c(r, t)$ can be written as

$$G(r, t) = N^{-1} \sum_i \langle c(r_i, t) c(r_i + r, t) \rangle, \tag{9}$$

where N is the total points in a system, and $\langle\ \rangle$ represents an ensemble average. The structure function is the Fourier transform of the spatial correlation function $G(r, t)$:

$$s(\boldsymbol{k}, t) = \sum_r \exp(i\boldsymbol{k} \cdot \boldsymbol{r}) G(\boldsymbol{r}, t), \tag{10}$$

which is directly proportional to the X-ray or neutron scattering intensity at a wave number transfer $\boldsymbol{k}$. It is convenient to introduce a normalized structure function $s(k, t)$,

$$s(k, t) = \sum_{[k]} s(\boldsymbol{k}, t) \Big/ \sum_{[k]} 1 \tag{11}$$

where the sum is over all values of $\boldsymbol{k}$ in the first Brillouin zone. It is suggested [19–21] that the normalized structure function has a scaling regime in which it behaves as:

$$s(k, t) = \kappa(t)^d F(x, t), \tag{12}$$

where k is the wave vector, $x = k/\kappa(t)$, t the time, $\kappa(t)$ a time-dependent length scale which behaves as $\kappa(t) \sim t^n$ for positive n. $F(x, t)$ is called the scaling function. In the scaling regime, $F(x, t) = F(x)$, which is independent of time.

Therefore, the dynamic scaling of a system can be determined by calculating the scaling function of the system. If the shape of scaling function does not change with time, it means that the system has reached the scaling state or steady state. Following the formulations of Lebowitz et al. [19], the structure functions and scaling functions are calculated for systems with different volume fractions of the coarsening phase. The time dependence of the structure function with 50% coarsening phase is shown in Fig. 3 as an example. It can be seen that the peak of the structure function increases as time increases and moves to smaller wave number k. Since the peak position $k_m(t)$ is related to the length scale of real space as $k_m(t) \sim 1/R(t)$, the decrease of $k_m(t)$ indicates the increase of grain size in real space. Therefore, the time dependence of $k_m(t)$ can also be used to study the coarsening kinetics. We found that this method works well for the case of 50% of each phase. However, when the volume fraction departs from 50%, say for 90% coarsening phase, the structure function has a large tail in the large k regime, which affects the accuracy of the kinetics calculated from structure functions. Therefore, we still utilize the real space method to extract the coarsening kinetics. The calculated scaling function for 50% and 90% of coarsening phase are shown in Figs. 4 and 5 as examples. It is obvious that scaling functions are independent of time for all volume fractions shown, indicating that these systems have reached the steady state after a short transient time. The scaling functions in other volume fractions are similar to Figs. 4 and 5 and all systems scale after a short transient

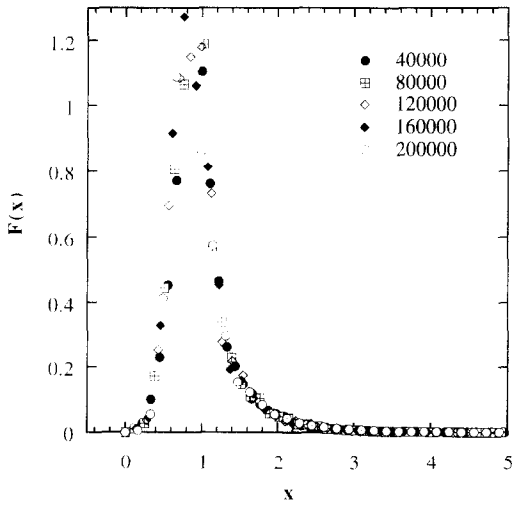

Fig. 4. The relations of the scaling function $F(k, t)$ with the normalized wave number x ($x = k/\kappa(t)$) in the reciprocal space at different time steps in 50% coarsening phase system. Time step = 40000, 80000, 120000, 160000, and 200000.

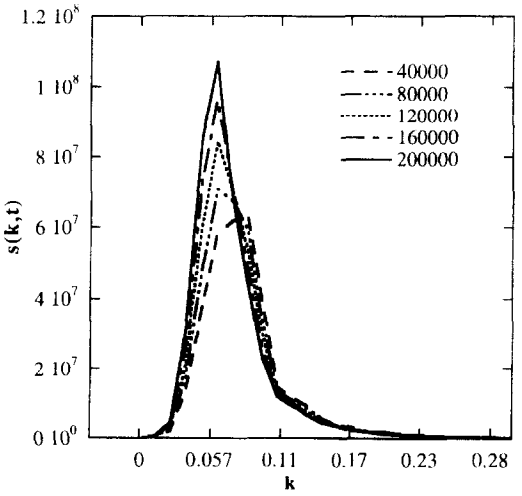

Fig. 3. The relations of the structure function $s(k, t)$ with the wave number k in the reciprocal space at different time steps in 50% coarsening phase system. Time step = 40000, 80000, 120000, 160000, and 200000.

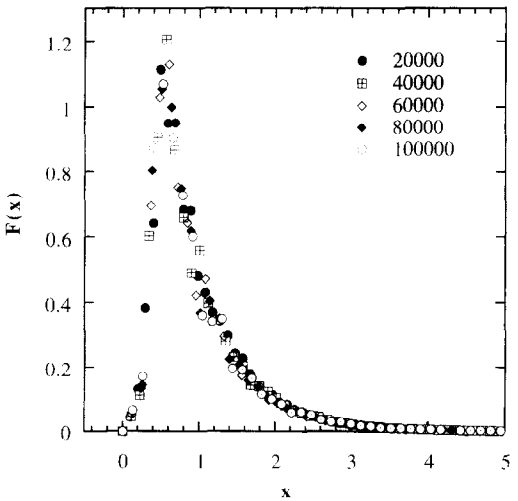

Fig. 5. The relations of the scaling function $F(x, t)$ with the normalized wave number x ($x = k/\kappa(t)$) in the reciprocal space at different time steps in 90% coarsening phase system. Time step = 20000, 40000, 60000, 80000, and 100000.

time. Hence, the studies of scaling function give confidence in the kinetic data extracted from these simulations.

The time dependencies of average grain size in systems with 25% and 90% of coarsening phase are shown in Figs. 6 and 7. In these plots, the solid lines are the non-linear fits to the power growth law $R_t^m - R_0^m$ with three variables m, k and R_0. It is found that these data fit power growth law very well with $m = 3$ in all cases, even for the very high volume fraction of coarsening phase (90%). It is clear that the shape accommodation of particles will not affect the growth exponent m as long as the system is in the scaling regime. Even though the growth exponent is independent of the volume fraction of the coarsening phase, the kinetic coefficient k is strongly volume-fraction dependent. The dependence of the kinetic coefficient k on the volume fraction of coarsening phase is shown in Fig. 8. At 25% coarsening phase, the kinetic coefficient k is 0.833, while at 90% coarsening phase, the coefficient increases to 24.45 which is about 30 times higher than that in the 25% system. The rapid increase in the kinetic coefficient k can be attributed to the dramatic decrease of the diffusion distance of atoms in the matrix phase, as the volume fraction of coarsening phase increases. At low volume fraction (25%), the typical diffusion distance is the mean spacing between particles which is much larger than the grain boundary thickness. At 90% coarsening phase, it can be seen from microstructures (Fig. 2) that the typical diffusion distance between grains becomes comparable with the grain boundary width, which will greatly enhance the coarsening kinetics.

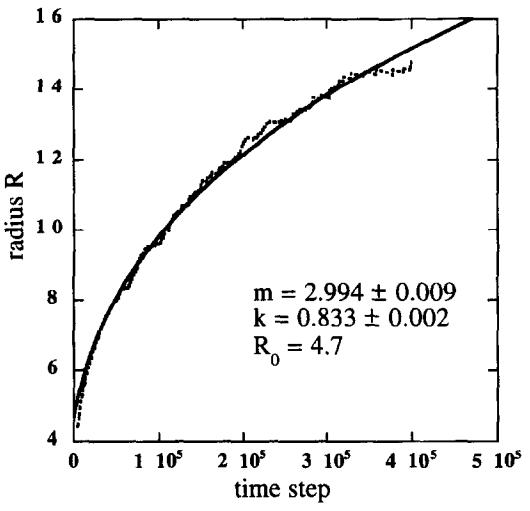

Fig. 6. The time dependence of the average grain size of the coarsening phase in the 25% coarsening phase system. The dots are the measured data from simulated microstructures. The solid line is a non-linear fit to the power growth law $R_t^m - R_0^m = kt$ with three variables m, k and R_0.

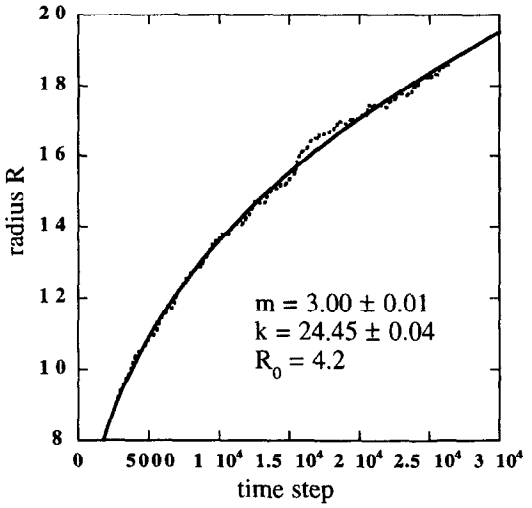

Fig. 7. The time dependence of the average grain size of the coarsening phase in the 90% coarsening phase system. The dots are the measured data from simulated microstructures. The solid line is a non-linear fit to the power growth law $R_t^m - R_0^m = kt$ with three variables m, k and R_0.

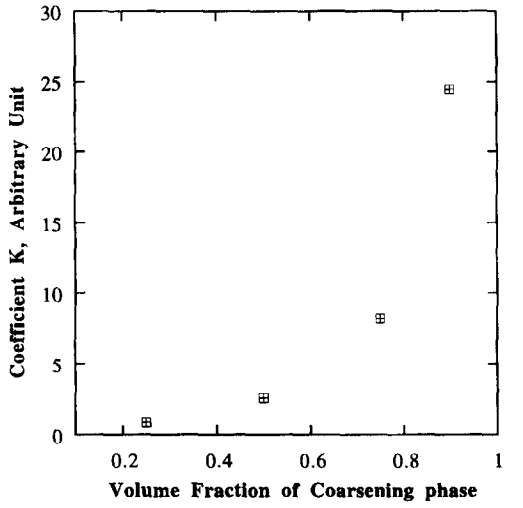

Fig. 8. The dependence of the kinetic coefficient k on the volume fraction of the coarsening phase.

4. Summary

A computer simulation model for modeling Ostwald ripening in two-phase systems has been constructed by using continuum field theory. The microstructural evolution and the kinetics of Ostwald ripening can be studied by numerically solving the time-dependent Ginzburg–Landau (TDGL) equations. The simulated microstructures are in a striking resemblance with those experimental observations. The shape accommodation of second phase particles occurs as the volume fraction increases. It was observed that scaling functions are independent of time for all volume fractions after a short transient time, indicating that these two-phase systems reach the steady state or scaling state. It was found that the coarsening kinetics of second phase particles follows the power growth law $R_t^m - R_0^m = kt$ and the growth exponent $m = 3$ is independent of the volume fraction of the coarsening phase and the details of the microstructures. The kinetic coefficient k increases dramatically as the volume fraction of the coarsening phase increases.

Acknowledgements

D.F. and S.P.C.'s work is supported by the U.S. Department of Energy, Division of Materials Science, Office of Basic Energy Science, and L.-Q.C.'s work is supported by the National Science Foundation under the grant number DMR 96-33719 and P.W.V.'s work is supported by Office of Naval Research. Computer simulations were performed at the Pittsburgh Supercomputing Center and the Advanced Computing Laboratory at Los Alamos National Laboratory.

References

[1] I.M. Lifshitz, V.V. Slyozov, J. Phys. Chem. Solids 19 (1961) 35.
[2] C. Wagner, Z. Elektrochem. 65 (1961) 581.
[3] A.J. Ardell, Phase Transformations '87, Inst. Metals, London, 1987, p. 485.
[4] R.M. German, Liquid Phase Sintering, Plenum Press, New York, NY, 1985, pp. 133–138.
[5] P.W. Voorhees, Annu. Rev. Mater. Sci. 22 (1992) 197, and references therein.
[6] A.J. Ardell, Acta Metall. 20 (1972) 61.
[7] K. Tsumuraya, Y. Miyata, Acta Metall. 31 (1983) 437.
[8] A.D. Brailsford, P. Wynblatt, Acta Metall. 27 (1979) 489.
[9] Z. Fang, B.R. Patterson, M.E. Turner, Acta Metall. 40 (1992) 713.
[10] C.W.J. Beenakker, Phys. Rev. A 33 (1986) 4482.
[11] A.J. Ardell, Phys. Rev. B 41 (1990) 2554.
[12] A. Chakrabarti, R. Toral, J.D. Gunton, Phys. Rev. E 47 (1993) 3025.
[13] J.H. Yao, K.R. Elder, H. Guo, M. Grant, Phys. Rev. B 45 (1992) 8173.
[14] V. Tikare, Numerical Simulation of Grain Growth in Liquid Phase Sintered Materials, Ph.D. Thesis, Case Western Reserve University, December, 1994.
[15] D. Fan, L.-Q. Chen, Acta Mater. 45 (2) (1997) 611.
[16] D. Fan, L.-Q. Chen, Acta Mater. 45 (3) (1997) 1115.
[17] L.-Q. Chen, D. Fan, J. Am. Ceram. Soc. 79 (1996) 1163.
[18] D. Fan, L.-Q. Chen, Diffusion-Controlled Grain Growth in Two-Phase Solids, Acta Mater. 45(8) (1997) 3297.
[19] J.L. Lebowitz, J. Marro, M.H. Kalos, Acta Metall. 30 (1982) 297.
[20] Y. Oona, S. Puri, Phys. Rev. Lett. 58 (1987) 836.
[21] Y. Enomoto, R. Kato, J. Phys.: Condens. Matter 2 (1990) 9215.